Engineering hydrogels with homogeneous mechanical properties for controlling stem cell lineage specification

Bin Xue[a,1] (ID), Dehua Tang[b,1] (ID), Xin Wu[a], Zhengyu Xu[a], Jie Gu[a], Yueying Han[a], Zhenshu Zhu[a], Meng Qin[a], Xiaoping Zou[b] (ID), Wei Wang[a,c], and Yi Cao[a,c,d,e,2] (ID)

[a]Collaborative Innovation Center of Advanced Microstructures, National Laboratory of Solid State Microstructure, Key Laboratory of Intelligent Optical Sensing and Manipulation, Ministry of Education, Department of Physics, Nanjing University, Nanjing 210093, China; [b]Department of Gastroenterology, Nanjing Drum Tower Hospital, Affiliated Drum Tower Hospital, Medical School of Nanjing University, Nanjing 210008, China; [c]Institute for Brain Sciences, Nanjing University, Nanjing, 210093, China; [d]Chemistry and Biomedicine Innovation Center, Nanjing University, Nanjing, 210093, China; and [e]Wenzhou Institute, University of Chinese Academy of Sciences, Wenzhou 325001, China

The extracellular matrix (ECM) is mechanically inhomogeneous due to the presence of a wide spectrum of biomacromolecules and hierarchically assembled structures at the nanoscale. Mechanical inhomogeneity can be even more pronounced under pathological conditions due to injury, fibrogenesis, or tumorigenesis. Although considerable progress has been devoted to engineering synthetic hydrogels to mimic the ECM, the effect of the mechanical inhomogeneity of hydrogels has been widely overlooked. Here, we develop a method based on host–guest chemistry to control the homogeneity of maleimide–thiol cross-linked poly(ethylene glycol) hydrogels. We show that mechanical homogeneity plays an important role in controlling the differentiation or stemness maintenance of human embryonic stem cells. Inhomogeneous hydrogels disrupt actin assembly and lead to reduced YAP activation levels, while homogeneous hydrogels promote mechanotransduction. Thus, the method we developed to minimize the mechanical inhomogeneity of hydrogels may have broad applications in cell culture and tissue engineering.

hydrogel | mechanical homogeneity | host–guest chemistry | stem cell | differentiation

In tissues, cells reside in a complex extracellular microenvironment whose mechanical properties often vary both in space and in time during regular tissue homeostasis or disease development (1). Growing evidence suggests that changes in local mechanical properties can have a considerable impact on cell fate (2–6, 7–13). For example, the intricate local mechanical environment can strongly affect wound healing and tissue regeneration (14, 15). In synthetic biomaterials (e.g., hydrogels) that are used for cell culture and tissue engineering, the mechanical heterogeneity is also ubiquitous although, in many cases, undesirable (10, 16–22). For hydrogels prepared by the polymerization of monomers, variations in local monomer concentrations and the heat released from the chemical reactions can lead to various defects in the hydrogel network. For hydrogels prepared by the chemical crosslinking of polymers, the broad distribution of the molecular weight of the polymers and their nonuniform mixing before gelation can also cause dramatic variation in the local mechanical properties. Although the effect of the overall mechanical properties of hydrogels on cell behaviors has been widely explored, how mechanical heterogeneity at the nanoscale affects cell behaviors remains poorly understood.

A major obstacle in addressing this question is the synthesis of hydrogels with uniformly distributed mechanical properties. By coupling four-armed poly(ethylene glycol) (PEG) macromers with narrowly distributed molecular weights, Sakai and coworkers have shown that it is possible to prepare hydrogels with minimal structural defects (23). The chemical reactions that are widely used for gelation include click chemistry (24, 25), amine-active ester reactions (26), maleimide–thiol conjugation (27, 28),

and thiol-ene reactions (29, 30). The maleimide–thiol reaction is of special interest because it takes place under mild conditions, requires no catalysis, and does not generate small-molecule byproducts (27, 31–34). The hydrogels prepared by maleimide–thiol reaction have been widely used for organoid generation (35), protein and cell delivery (36), and controlled release (37). However, this reaction is too fast to allow adequate mixing of the macromer solution, leading to heterogeneous gelation. Because of variation in the crosslinking density, hydrogels often contain microdomains with distinct mechanical properties (38, 39). A few methods have been developed to minimize hydrogel heterogeneity by slowing this reaction, including lowering the gelation pH, changing the local pK_a of thiol, or adding thiol-binding metal ions (38, 40–43). However, these methods often require nonphysiological gelation conditions or lead to only limited improvement.

In this work, we introduced host–guest chemistry to slow down the maleimide–thiol reaction for hydrogel preparation. We discovered that maleimide can form a complex with β-cyclodextrin

Significance

Hydrogels are extensively used for cell culture, tissue engineering, and flexible electronics. In all of these applications, mechanical properties of hydrogels play an important role. Although tremendous studies have been devoted to optimizing the stiffness, strain, toughness, and dynamic mechanical response, the mechanical homogeneity of hydrogels has rarely been considered. By developing a general strategy to control the mechanical homogeneity of hydrogels, here we show that nanoscale variation in matrix stiffness can considerably affect the lineage specification of human embryonic stem cells. Inhomogeneous hydrogels suppress mechanotransduction and facilitate stemness maintenance, while homogenous hydrogels promote mechanotransduction and osteogenic differentiation. Therefore, engineering hydrogels with controllable and well-defined nanoscale homogeneity may have considerable implications in stem cell culture and regenerative medicine.

(β-CD), lowering the free maleimide concentrations in the gelation system. We showed that the four-armed PEG hydrogels prepared using this approach possessed fewer network defects and more uniform mechanical properties. Moreover, we revealed that mechanical homogeneity can considerably affect the lineage specification of human embryonic stem cells (hESCs). We proposed that this effect can be attributed to the disruption of the assembly of actin fibers and the subsequent mechanotransduction pathways. We anticipate that this method can greatly improve the mechanical homogeneity of many cell culture systems to better regulate stem cell lineage specification.

Results

Reducing Gelation Speed by Host–Guest Chemistry between Maleimide and β-CD. We decided to use β-CD as the potential guest molecule to shield maleimide from thiol groups in the pregel solution and thus decrease the gelation rate. The concept is illustrated in Fig. 1. β-CD is one of the most widely studied hosts in supramolecular chemistry (44–49), with an inner cavity of 6.1 Å, slightly larger than the diameter of maleimide (4.8 to ~5.4 Å). The comparable size of the inner cavity of β-CD and the size of maleimide leads to the formation of the lock-and-key–type structural relationship. Moreover, the succinimide ring of maleimide is relatively hydrophobic and can bind with the inner cavity of β-CD through the hydrophobic effect. Once the host–guest complex is formed, the succinimide ring of maleimide becomes inaccessible to the thiol groups (Fig. 1A). The reaction-free energy diagram explains the effect of the formation of the β-CD−maleimide complex on the maleimide–thiol reaction rate in detail (Fig. 1B). The reaction of maleimide and thiol is fast with a low activation barrier (ΔG). This activation barrier is considerably increased when maleimide forms complexes with β-CD. The increase of the free energy barrier equals the free energy for the formation of the complex (ΔG_{eq}), which is determined by the binding constant of the β-CD−maleimide complex and the β-CD concentration. Therefore, by adding a suitable amount of β-CD, we expected to make the hydrogels formed by mixing thiol- and maleimide-terminated 4-armed PEG (Mw: 20 kDa, named PEG-SH and PEG-Mal, respectively) more uniform due to the reduced gelation rate (Fig. 1 C and D).

We next measured the binding free energy of β-CD and maleimide using isothermal titration calorimetry (ITC) by titrating β-CD into the PEG-Mal solution (Fig. 2A). The binding constant (K_a) was ~6.66×10^4 M^{-1}. The binding stoichiometry was estimated to be ~1.0 (1/0.995), suggesting the formation of a 1:1 complex. We further studied how complexation with β-CD affects the maleimide–thiol reaction rate by monitoring this reaction through the ultraviolet-visible (UV-vis) adsorption of the maleimide group. We mixed PEG-Mal and PEG-SH and observed a decrease in UV adsorption at ~300 nm as the reaction proceeded (*SI Appendix*, Fig. S1), indicating the conversion of maleimide to maleimide–thiol adducts that do not absorb UV in this region. The generation of maleimide–thiol conjugates at different β-CD:PEG-Mal ratios is shown in the top panel of Fig. 2B. The reaction clearly slowed down as the β-CD concentration increased. Moreover, the reaction kinetics were theoretically predicted based on the second-order reaction rate equation using the experimentally determined β-CD−maleimide binding constant (Fig. 2B, *Bottom*). The theoretical prediction semiquantitatively replicated the experimental results, confirming the proposed mechanism.

Characterization of the Mechanical Homogeneity of the Hydrogels. We then prepared hydrogels by mixing equimolar PEG-Mal and PEG-SH in the presence of various ratios of β-CD. The inhomogeneity of the crosslinking can be studied by monitoring the residual thiol groups using a turn-on fluorescence probe (50), whose fluorescence intensity is enhanced by more than 100 times upon reacting with thiol. After removing the unreacted fluorescent probes, the hydrogels were scanned using laser confocal fluorescence microscopy to detect the spatial distribution of the unreacted thiol groups (*SI Appendix*, Fig. S2). The fluorescent spots, which could also be considered defects in the hydrogel network, were greatly decreased in hydrogels prepared in the presence of β-CD. Although confocal fluorescence microscopy
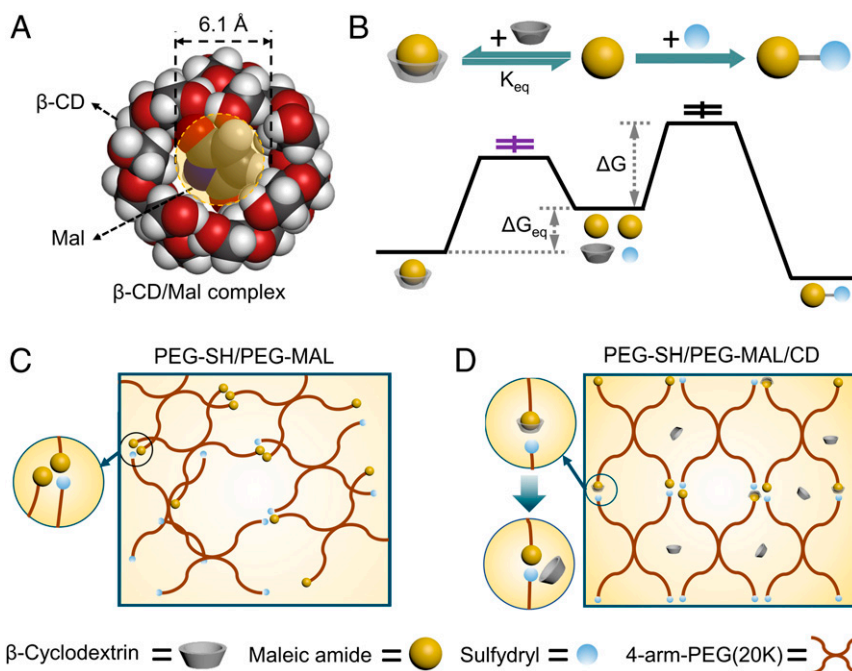
Fig. 1. Reducing the gelation speed and generating a homogeneous hydrogel using host–guest chemistry between maleimide and β-CD. (A) Schematic of the β-CD–maleimide complex. (B) Schematic and free energy diagram of the effect of the β-CD–maleimide complex on the maleimide–thiol reaction. (C and D) Schematic of the hydrogel networks formed in the absence (C) and presence (D) of β-CD.
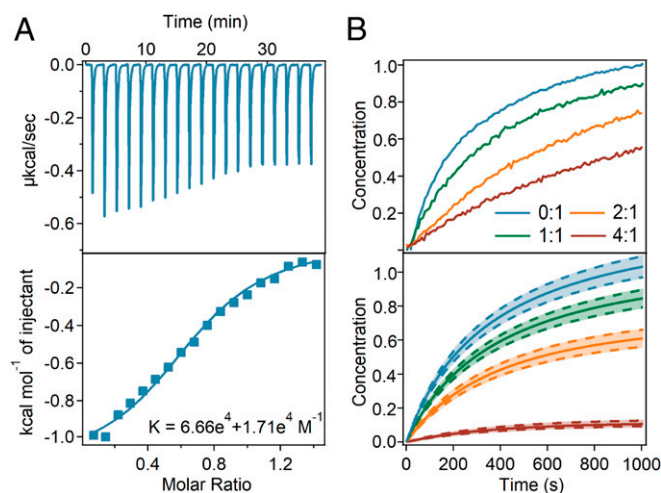
Fig. 2. Binding between β-CD and maleimide affects the maleimide–thiol reaction kinetics. (*A*) The binding affinity of β-CD and PEG-Mal was determined using ITC by titrating the β-CD solution into a solution of four-armed PEG-Mal. (*B*) Measured (*Top*) and calculated (*Bottom*) reaction kinetics of four-armed PEG-Mal and four-armed PEG-SH at different ratios of β-CD and PEG-Mal (0:1, 1:1, 2:1, and 4:1) monitored by UV spectroscopy over time at 25 °C. The dotted lines indicate the amplitude of the calculated reaction kinetics.

can greatly reduce the excitation and detection volume compared with epi-fluorescence microscopy, it still suffers from blurring when imaging hydrogel samples with stacked fluorescent dyes along the *z*-axis, leading to a relatively bright background. The average brightness, density, and area of the fluorescence spots calculated from the projected images in the *z*-axis direction of the hydrogels were approximately two to four times higher in the hydrogels without β-CD than in the hydrogels with β-CD (*SI Appendix*, Fig. S3). The optimal β-CD:PEG-Mal ratio was 1:1, and higher β-CD ratios also introduced additional defects, possibly due to competition with the maleimide-thiol reaction decreasing the reaction efficiency. We also used 5,5′-dithiobis-(2-nitrobenzoic acid) (51) to quantify the unreacted thiol remaining in the hydrogels, and the results were consistent with those from

the fluorescence measurements (*SI Appendix*, Fig. S4). It is worth mentioning that β-CD can be almost completely removed from hydrogels by dialyzing against water. The amount of β-CD washed out was ~98.2% of that added during gelation (*SI Appendix*, Fig. S5). These measurements suggested that β-CD−maleimide host−guest chemistry can increase the homogeneity of the hydrogel network by slowing down the reaction kinetics without introducing additional chemical modifications to the hydrogels.

We then studied the mechanical homogeneity of the hydrogels by measuring the local mechanical properties using indentation based on atomic force microscopy (IT-AFM) at submicrometer spatial resolution. As shown in Fig. 3*A*, the hydrogel films were allowed to swell to equilibrium in water and then mounted on a glass substrate before the measurement. The cantilever approached the surface of hydrogels at a constant speed of 2 $\mu m \cdot s^{-1}$ and then retracted (Fig. 3*B*). The Young's modulus of the hydrogel at a given position was calculated by fitting the approaching traces using the Hertz model. Representative elasticity maps (40 × 40 pixels) of hydrogel surfaces prepared at different β-CD:PEG-Mal ratios are shown in Fig. 3 *C–F*. The spatial variation in the Young's modulus was clearly more pronounced for the hydrogels prepared without β-CD than those prepared with β-CD. The distributions of the local Young's modulus in each hydrogel are summarized in the inset of Fig. 3 *C–F* and *SI Appendix*, Fig. S6 *A–D*. The Young's moduli for the hydrogel with β-CD:PEG-Mal ratios of 0:1, 1:1, 2:1, and 4:1 were 79.3 ± 24.2, 92.4 ± 12.7, 86.9 ± 10.9, and 83.6 ± 15.2 kPa, respectively. The addition of β-CD led to slightly higher overall Young's moduli and narrower distributions. Both effects can be explained by the improved network homogeneity. Furthermore, the widths of modulus histograms obtained from the two-dimensional Young's modulus images at the β-CD:PEG-Mal ratio of 1:1 was smaller than those at the other ratios, indicating the highest mechanical homogeneity (*SI Appendix*, Fig. S6*E*). Moreover, similar distributions of Young's modulus were observed in hydrogels prepared using different PEG concentrations with the Young's modulus at a wide range of ~19 to 115 kPa (*SI Appendix*, Figs. S7–S10). The macroscopic mechanical properties of the hydrogels measured by compressive mechanical tests showed the same trend of Young's moduli (*SI Appendix*, Figs. S11–S13). The swelling ratios, porosity, and microstructures of all the hydrogels were almost the same, indicating that the bulk physical properties were not affected by the
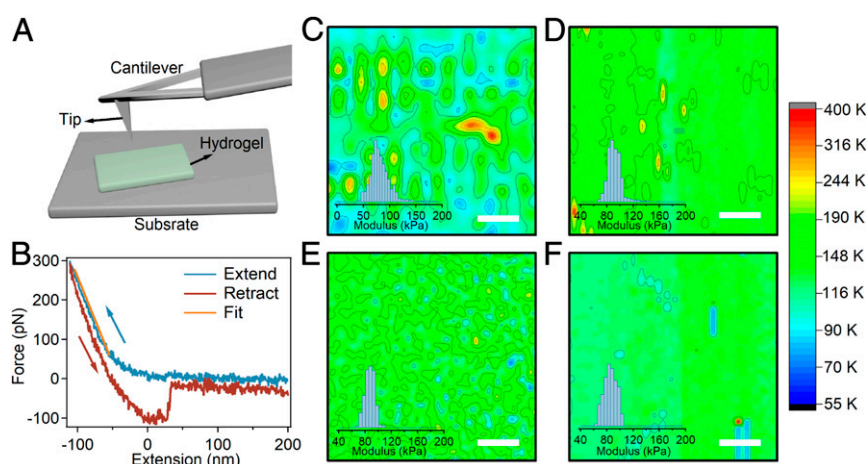
Fig. 3. Mechanical homogeneity of the hydrogels prepared in the presence of β-CD. (*A*) Schematic illustration of the IT-AFM experiments on hydrogel samples. The hydrogel was spread onto a glass coverslip and immersed in pure water for the AFM measurement. The cantilever tip was extended into the hydrogel sample and retracted to obtain the force–distance trace at each spot, from which the elasticity was deduced using the Hertz model. (*B*) Representative force–distance traces on hydrogels. The hysteresis between "extend" and "retract" traces is due to sample deformation and the adhesion between the cantilever tip and the hydrogel. The red line corresponds to the fitting of the contact region in the "extend" trace using the Hertz model. (*C–F*) Two-dimensional Young's modulus distributions of hydrogel surfaces determined by AFM at β-CD and PEG-Mal ratios of 0:1 (*C*), 1:1 (*D*), 2:1 (*E*), and 4:1 (*F*). (Scale bar, 1 μm.) Insets correspond to typical histograms of Young's modulus.

Xue et al.
Engineering hydrogels with homogeneous mechanical properties for controlling stem cell lineage specification

PNAS | 3 of 9
https://doi.org/10.1073/pnas.2110961118

addition of β-CD (*SI Appendix*, Figs. S14 and S15). All these results suggest the successful generation of homogeneous hydrogels by slowing down the maleimide–thiol reaction kinetics through β-CD−maleimide host–guest chemistry. We chose the optimal β-CD:PEG-Mal ratio of 1:1 for the subsequent cell culture studies. The inhomogeneous hydrogels prepared without β-CD and the homogenous hydrogels with β-CD are hereafter termed I-gels and H-gels, respectively.

Effect of Homogeneity on the Stemness Maintenance and Differentiation of hESCs. Before culturing hESCs on these hydrogels, we studied the biocompatibility of the hydrogels using 7721 and HK-2 cells. The viabilities of both cell lines were greater than 80% after culturing for 24 h on the hydrogels, as

determined using CellTiter-Glo Reagent and live/dead cell staining (*SI Appendix*, Fig. S16). Note that the cells on the H-gels showed similar viabilities to those on the I-gels, indicating that involving β-CD in the hydrogel preparation did not affect the biocompatibility. Next, we studied the effect of hydrogel homogeneity on the differentiation of hESCs cultured on the two types of hydrogels. Hydrogels were prepared in 12-well cell culture plates, and wells (glass surface) without hydrogels were used as controls. We also added 0.2 mg · mL^{-1} cRGD (Cyclo[Arg-Asp-D-Phe-Cys]) to the hydrogel mixture before gelation to facilitate cell attachment. The hydrogels were swelled to equilibrium, and then hESCs were seeded at a density of 1×10^3 cell colonies per well in mTeST1 according to manufacturer's instructions. The medium was replaced daily. After the cells were
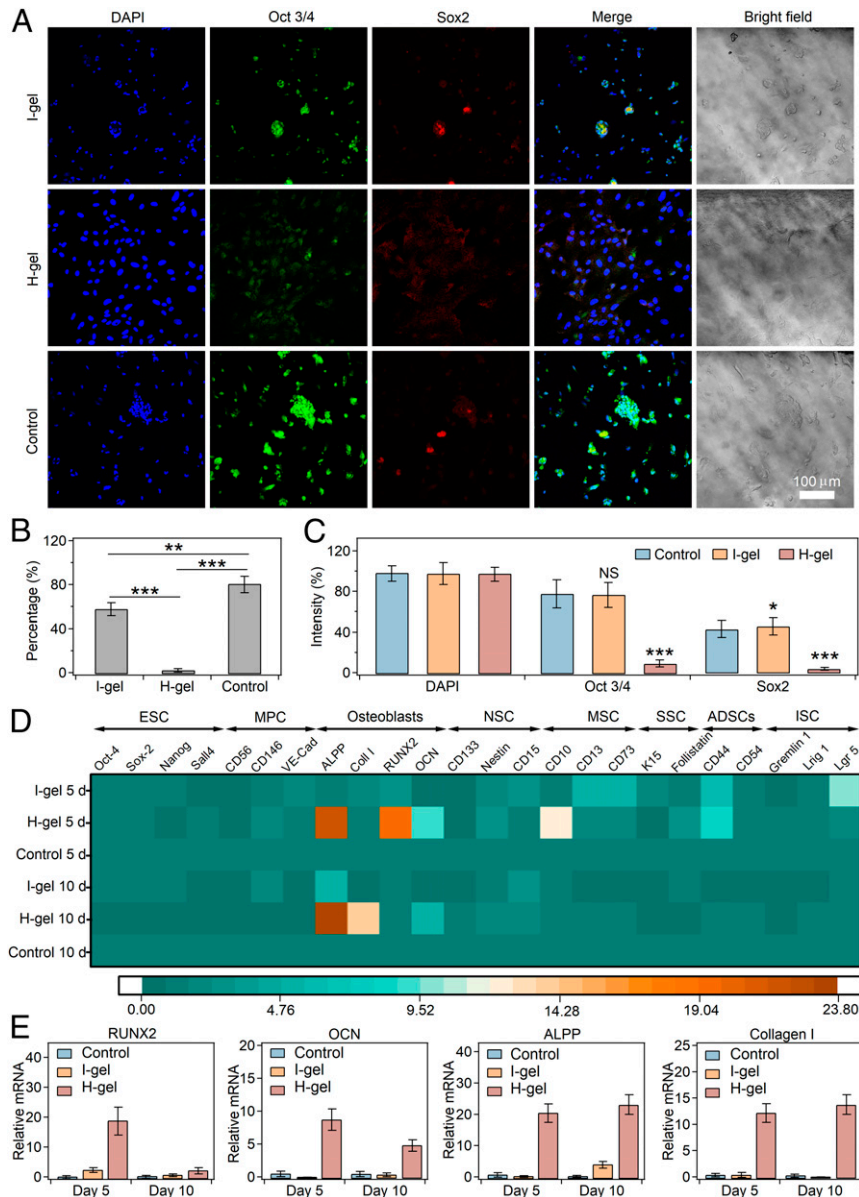
Fig. 4. Stemness maintenance and differentiation of hESCs cultured on H-gels and I-gels. (*A*) hESCs identified by molecular marker immunostaining after culture for 10 d on different surfaces. hESCs on the cell culture wells were set as the control group. Oct3/4 (red) and Sox2 (green), specific markers for stemness maintenance, were down-regulated in H-gels. Cell nuclei are indicated by DAPI (Blue). (*B*) Percentages of cells in cell aggregates on different substrates. **: $P < 0.01$; ***: $P < 0.001$. (*C*) Normalized fluorescence intensity of Oct3/4 and Sox2 with DAPI as the 100% for cells from the I-gel, H-gel, and control groups. NS: not statistically significant, $P > 0.05$; *: $P < 0.05$; and ***: $P < 0.001$. (*D*) Heat map of mRNA expression corresponding to various stem cell lines in hESCs after culture for 5 and 10 d on different substrates. (*E*) mRNA expression of RUNX2, OCN, ALP, and collagen I in hESCs after culturing for 5 and 10 d on different substrates.

cultured for 10 d, the cell aggregates and stemness of hESCs were identified by immunostaining for the molecular markers Oct3/4 and Sox2, two important transcription factors that maintain the self-renewal and pluripotency of hESCs (Fig. 4A). In terms of cell aggregates, hESCs adhered to both the hydrogels and the control glass substrate well but showed distinct morphologies. hESCs on the I-gels remained as cell aggregates, and only small numbers of cells separated and spread on the gels. In contrast, almost all the hESCs grew separately and adopted a spreading conformation on the H-gels. The percentages of cells remaining as cell aggregates on the I-gels, the H-gels, and the glass substrates were 59.4, 5.0, and 81.7%, respectively (Fig. 4B). In terms of cell stemness, both Oct3/4 and Sox2 were significantly decreased in cells on the H-gels compared with those on the I-gels or glass substrates, indicating that homogeneous hydrogels might reduce stemness and promote the differentiation of hESCs. Fluorescent quantitative analysis also supported this finding (Fig. 4C). The fluorescence intensities of Oct3/4 and Sox2 for hESCs on the H-gels were only 11.6 and 6.7% of the intensities of DAPI, respectively, while those on the I-gels were much higher (>40%),
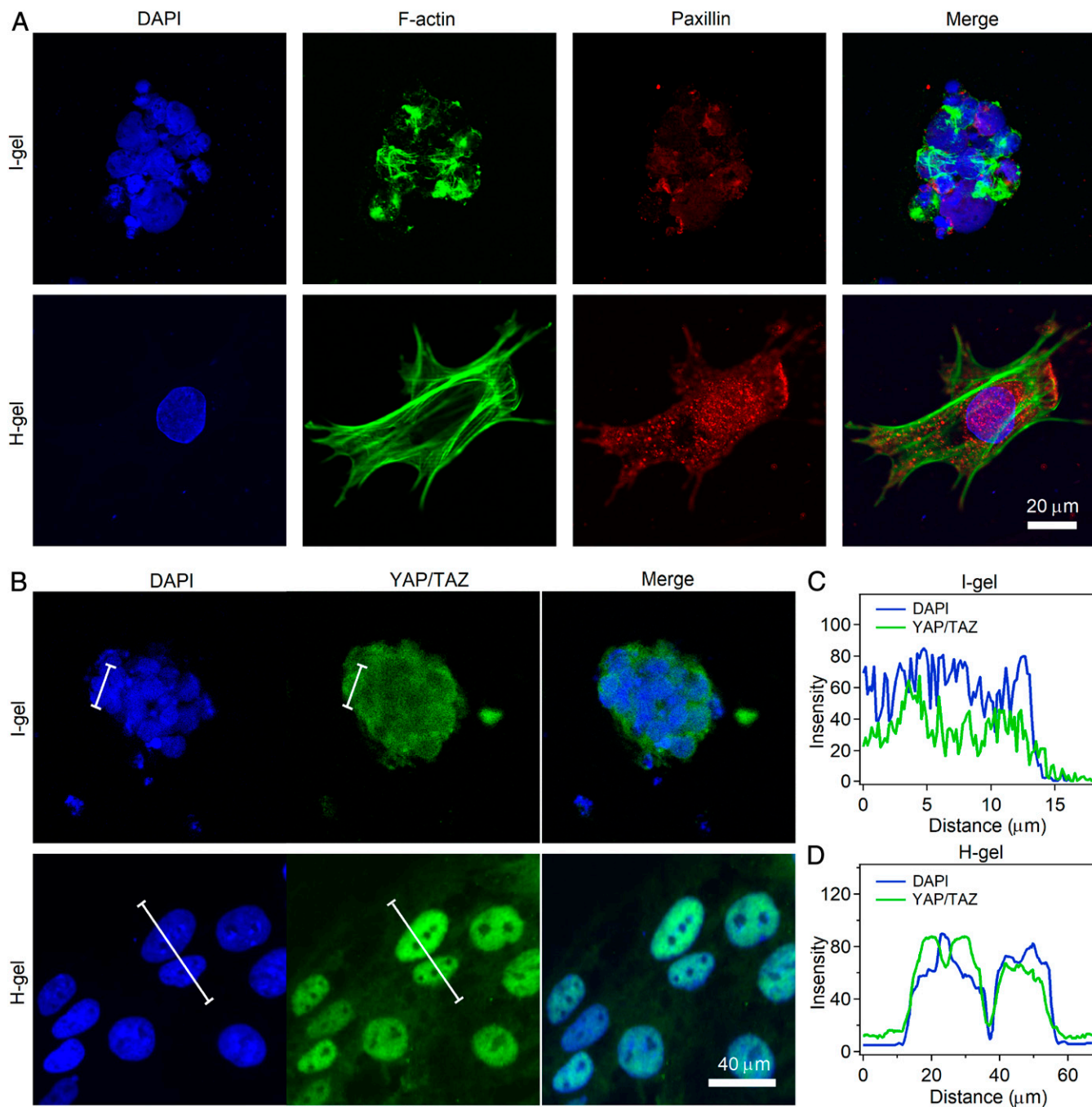
Fig. 5. Mechanical homogeneity of hydrogels affects the mechanotransduction pathways of hESCs. (A) Immunostaining of nuclei (DAPI, blue), F-actin (phalloidin, green), and adhesion plaques (paxillin, red) of hESCs on I-gels and H-gels. (Scale bar, 20 μm.) (B) Immunostaining of nuclei (DAPI, blue) and YAP/TAZ (green) of hESCs cultured on I-gels and H-gels. (Scale bar, 40 μm.) (C and D) Intensity profiles (line regions in B) of DPAI and YAP/TAZ are more correlated on the H-gels (D) than on the I-gels (C).

Xue et al.
Engineering hydrogels with homogeneous mechanical properties for controlling stem cell lineage specification

PNAS | 5 of 9
https://doi.org/10.1073/pnas.2110961118

similar to those on the glass substrates, further confirming the enhanced differentiation of hESCs on H-gels. The overall Young's moduli of the H-gels were slightly higher than those of the I-gels. We then studied whether this difference in Young's moduli affected the stemness of hESCs. By varying the polymer concentrations, we obtained H-gels and I-gels with both higher Young's moduli of ~115 kPa and lower Young's moduli of ~60 kPa (*SI Appendix*, Figs. S9 and S10). The molecular marker immunostaining gave consistent results irrespective of the small variations in the Young's modulus (*SI Appendix*, Figs. S17 and S18). These results indicate that the homogeneity of the hydrogels can considerably affect the differentiation and stemness maintenance of stem cells.

We also performed additional experiments to exclude other possible causes of the distinct differentiation behaviors of hESCs on the I-gels and the H-gels. Previous studies have suggested that surface roughness can also affect stem cell differentiation. To exclude this possibility, we measured the roughness of both the I-gels and the H-gels. They showed identical roughness of ~30 nm (*SI Appendix*, Fig. S19). Ligand distribution has also been reported to affect stem cell lineage specification. The distribution of cRGD on the hydrogels is difficult to determine directly. As an alternative, we used a thiol-containing fluorescent dye (Cy5-PEG-SH, 2 kDa) to mimic the ligand coupling process. Our results indicated that the fluorescent dye was evenly distributed on both the I-gels and the H-gels (*SI Appendix*, Fig. S20A). The variation in fluorescence intensity was less than 5% (*SI Appendix*, Fig. S20B). We expected that cRGD would be homogenously distributed on both the I-gels and the H-gels, because it was coupled to the hydrogels through the same reaction. Moreover, the stress–relaxation behaviors were similar for all the hydrogels at different ratios of β-CD and PEG-Mal, ruling out the effects of stress–relaxation properties on the differentiations of the hESCs (*SI Appendix*, Fig. S21). As a residual amount of β-CD may still be present in the H-gels (<72 μg · mL^{-1}), we then studied whether β-CD could affect hESC differentiation. We added additional β-CD (up to 3 mg · mL^{-1}) to the control groups, and the cell morphology and stemness were not affected (*SI Appendix*, Fig. S22). These studies confirm that mechanical homogeneity is the major factor that determines the differentiation of hESCs.

We further studied the lineage specification of hESCs using qRT-PCR. As shown in *SI Appendix*, Table S1, 25 well-established markers were used in the experiments (ESC: Oct-4, Sox-2, Nanog, and Sall4; myogenic precursor cell: CD56 and CD146; VE-cadherin; osteoblasts: ALPP, collagen I, RUNX2, and OCN; neural stem cell: CD133, nestin, and CD15; mesenchymal stem cell (MSC): CD10, CD13, and CD73; skin stem cell: K15 and follistatin; adipose-derived stem cell: CD44 and ICAM-1/CD54; intestinal stem cell: gremlin 1, Lrig 1, and Lgr 5). The relative gene expression levels are summarized in a two-dimensional diagram (Fig. 4D). Clearly, the expression levels of the marker messenger-ribonucleic acid (mRNA) of osteoblasts were significantly higher for the cells seeded on the H-gels than those on the I-gels and the control glass substrates. The relative mRNA levels of RUNX2, OCN, ALPP, and collagen I in the cells cultured on the H-gels for 5 or 10 d were clearly higher than in the other two groups (Fig. 4E). These results suggest that the homogeneity of the hydrogels can promote osteogenic differentiation.

Enhanced Mechanotransduction on the H-Gels. To understand the mechanism underlying the distinct cell fate commitments on homogeneous and I-gels, we studied the morphology, cytoskeleton structures, and adhesion plaque of the cells on both the I-gels and H-gels using molecular marker immunostaining (Fig. 5A). The average spreading area of the hESC nuclei differed sharply between the two types of hydrogels (Fig. 5A). The average nuclear area was ~122 and ~38 μm^2 on the H-gels and the I-gels, respectively (*SI Appendix*, Fig. S23A). The stressed actin bundles of the cells on the H-gels were longer and more organized than those

on the I-gels. As a quantitative indicator of cytoskeletal tension, the relative intensity of actin was examined by normalizing the actin area to the nuclear area, and the relative actin intensity was 17.3 for the H-gels but was only 2.1 for the I-gels (*SI Appendix*, Fig. S23B). Moreover, punctate paxillin was observed on the H-gels, indicating that they were clustered at the cell surface to form mature focal adhesions. In contrast, less and more diffusive paxillin was observed on the I-gels than on the H-gels (Fig. 5A). The relative paxillin intensity (paxillin area/nucleus area) was 3.5 on H gels and as low as 0.52 on I-gels (*SI Appendix*, Fig. S23C). All these results indicate that hESCs grown on the H-gels showed more efficient mechanotransduction than those grown on the I-gels.

We further investigated whether the mechanically sensitive transcriptional coactivators YAP/(yes-associated protein)/TAZ (transcriptional coactivator with PDZ-binding motif) were involved in gauging mechanical homogeneity sensing into genetic events and eventually affecting hESC differentiation. YAP/TAZ were mainly observed in the nuclei of the cells cultured on the H-gels (Fig. 5B, *Bottom*). In contrast, YAP/TAZ mainly remained inactive and located in the cytoplasm of the cells on the I-gels (Fig. 5B, *Top*). The fluorescence intensity profiles for YAP/TAZ and the nuclei at the cross section of the cells cultured on the two hydrogels further confirmed these findings (Fig. 5 C and D). The cells seeded on the H-gels exhibited an $88.5 \pm 6.1\%$ nuclear YAP/TAZ activation while that for cells seeded on the I-gels was mostly deactivated in the cytoplasm with only $16.5 \pm 5.9\%$ nuclear localization (*SI Appendix*, Fig. S23D). All these results indicated that hydrogel homogeneity promotes the activation of YAP/TAZ and thus further regulates hESC differentiation.

Discussion

The development of hydrogel technology has greatly expanded the scope of many biomedical fields, including cell culture, tissue engineering, flexible electronics, and even artificial skin. In all these applications, the mechanical properties of hydrogels play an important role. Although tremendous studies have been devoted to optimizing the stiffness, strain, toughness, and dynamic mechanical response, improving the mechanical homogeneity of hydrogels has rarely been studied. In this work, we provided a way to reduce the reaction rate of Michael-type addition between maleimide and thiol. We showed that the resulting hydrogels were mechanically homogenous at the nanoscale. As this method can decrease the number of defects in hydrogels, it can also improve other mechanical properties, such as stretchability and toughness. Moreover, the concept of using a kinetic trap to slow gelation is not limited to maleimide–thiol conjugation and can be easily extended to other reactions. We envisioned that this technique could have broad applications in hydrogel technology.

Although synthetic hydrogels have been widely used for stem cell culture and tissue engineering, their mechanical inhomogeneity is often overlooked. Here, we showed that heterogeneous mechanical properties can greatly influence the behaviors of hESCs, adding to the complexity of their mechanical cues. Unexpectedly, we found that I-gels were advantageous for stemness maintenance. Even in relatively stiff hydrogels (~80 kPa), hESCs remained as cell aggregates and did not differentiate for 10 d. This suggests a method for the in vitro expansion of hESCs using hydrogel substrates with heterogeneous mechanical properties. On the other hand, we found that H-gels can promote osteogenic differentiation. Therefore, to use hydrogel scaffolds for cartilage and bone regeneration, it is critical to improve the homogeneity of the hydrogels. In many fundamental studies of stem cells responding to mechanical signals, hydrogel homogeneity should also be considered, as it may complicate the interpretation of the results.

How surfaces with varied mechanical and geometrical patterns affect the differentiation of stem cells has also been studied previously. Anseth and coworkers (52) used a photodegradation

reaction to create micrometre-scale patterns of soft (~2 kPa) and stiff (~10 kPa) regions in PEG hydrogels. They found that evenly spaced patterns facilitated mechanotransduction and led to enhanced osteogenesis while random patterns led to inefficient mechanotransduction. Similarly, in our study, we showed that nanoscale variation in the mechanical properties of hydrogels could also considerably affect the formation of focal adhesion structures and tensile actin bundles, which enabled hESCs to retain stemness features. On the other hand, homogeneous hydrogels led to more efficient mechanotransduction and promoted osteogenesis. Given that the mechanoreceptors (i.e., integrins) are at the scale of less than 100 nm (53), it is reasonable to infer that nanoscale variation in mechanical features is sufficient to interfere with mechanosensing pathways. Interestingly, in studies by Dalby and coworkers (54) using randomized patterned ligands, they found that disordered patterns promoted cell adhesion and subsequent osteogenic differentiation, while ordered patterns did not. In another work by Chien, Jin, and coworkers (55), the size of the patterns was found to be the key in inducing differentiation into osteoblast-like cells. Later, Ding and coworkers showed that both matrix stiffness and nanoscale features can affect stem cell differentiation (56). Obviously, the effect of varied surface mechanical patterns is distinct from that of varied surface nanoscale patterns. However, they can be understood under the same canvas; that is, ECM organization can affect the mechanosignaling of stem cells, regulate cytoskeletal structures, and eventually lead to differences in gene transcription.

In summary, in this work, we report a method to minimize the mechanical heterogeneity of synthetic nonfouling maleimide–thiol cross-linked PEG hydrogels by reducing the gelation speed using host–guest chemistry. This method is general and can improve many mechanical features of the resulting hydrogels. Moreover, we show that nanoscale variation in matrix stiffness can considerably affect the lineage specification of hESCs, which has not been seriously considered in many current stem cell studies. Given that the organization of mechanical patterns in living tissues can be greatly affected by injuries and diseases, our results may improve our understanding of mechanotransduction during disease progression and wound healing. Moreover, engineered H-gels are especially useful for promoting osteogenic differentiation and should find broad applications in bone tissue regeneration.

Materials and Methods

ITC Titration. All titrations were performed using a Microcal ITC200 apparatus at 298 K. Four-armed PEG-Mal and β-CD were dissolved in phosphate-buffered saline (PBS, 10 mM, pH = 7.4) to concentrations of 0.66 mM and 0.06 mM. Then, the four-armed PEG-Mal solutions were added to the solutions of β-CD during the titrations. Blank titrations in PBS (10 mM, pH = 7.4) were performed, and the result was subtracted from the corresponding titrations to account for the effect of the dilution. The fitting was performed by using Origin software provided by Microcal.

Reaction Rate Determination. The reaction of four-armed PEG-SH and four-armed PEG-Mal was monitored by UV spectroscopy. The UV absorbance at 300 nm of the mixture of four-armed PEG-SH (400 μM) and four-armed PEG-Mal (400 μM) was recorded using a V550 (JASCO Inc.) spectrophotometer to monitor the decrease in the concentration of four-armed PEG-Mal during the gelation process of hydrogels. For the reaction rate of PEG-SH/PEG-Mal/β-CD hydrogels, the UV absorbance of the mixture containing four-armed PEG-SH, four-armed PEG-Mal, and β-CD, in which the molar ratios of β-CD and four-armed PEG-Mal were 0:1, 1:1, 2:1, and 4:1, was recorded at 300 nm. Then, the concentration of four-armed PEG-Mal and maleimide–thiol adducts was calculated according to the calibration curves based on UV absorbance. The cuvette width was 1 cm, and the bandwidth was set to 0.2 nm.

Theoretical Prediction of Reaction Kinetics. To calculate the reaction rate of maleimide and thiol based on the binding constant measured by ITC, the reaction rate can be described by Eqs. **1–3**, in which [SH] and [Mal] correspond to the concentrations of maleimide and thiol, respectively. [Mal·SH] corresponds to the concentration of the maleimide and thiol compound.

$$V = \frac{d[Mal \cdot SH]}{dt} = k_1([SH] - [Mal \cdot SH])([Mal] - [Mal \cdot SH]), \quad \text{[1]}$$

$$\int_0^{[Mal \cdot SH]} \frac{d[Mal \cdot SH]}{([SH] - [Mal \cdot SH])([Mal] - [Mal \cdot SH])} = \int_0^t k_1 dt, \quad \text{[2]}$$

$$\frac{1}{[SH] - [Mal]} ln \frac{[Mal]([SH] - [Mal \cdot SH])}{[SH]([Mal] - [Mal \cdot SH])} = k_1 t. \quad \text{[3]}$$

The concentrations of maleimide, β-CD, and the complex maleimide and β-CD (Mal·CD) at thermodynamic equilibrium in the mixture of maleimide and β-CD were determined as

$$k_a[CD][Mal] = [Mal \cdot CD], \quad \text{[4]}$$

where k_a is the association constant of maleimide and β-CD. The integral molar quantity of maleimide was equal to that of thiol (5), while that of β-CD was equal to that of thiol. K_2 corresponds to the molar ratio of β-CD and thiol:

$$[Mal \cdot CD] + [Mal] = [SH] \quad \text{[5]}$$

$$[Mal \cdot CD] + [CD] = k_2[SH] \quad \text{[6]}$$

$$k_a k_2[Mal][SH] + [Mal](k_a[Mal] + 1) = [SH] \quad \text{[7]}$$

$$[Mal] = \frac{-((k_2 - 1)k_a[SH] + 1) + \sqrt{((k_2 - 1)k_a[SH] + 1)^2 + 4k_a[SH]}}{2k_a}$$
$$= \Psi([SH]). \quad \text{[8]}$$

In summary, the concentration of [Mal·SH] in the system at time t can be described by the following equation:

$$\frac{1}{[SH] - \Psi([SH])} ln \frac{\Psi([SH])([SH] - [Mal \cdot SH])}{[SH](\Psi([SH]) - [Mal \cdot SH])} = k_1 t, \quad \text{[9]}$$

$$[Mal \cdot SH] = \Psi([SH]) - \frac{\Psi([SH])([SH] - \Psi([SH]))}{[SH]e^{k_1 t([SH] - \Psi([SH]))} - \Psi([SH])}. \quad \text{[10]}$$

The generation of [Mal·SH] versus time at different ratios of β-CD and four-armed PEG-Mal (0:1, 1:1, 2:1, and 4:1) was calculated and is shown at the bottom of Fig. 2B.

Preparation of PEG-SH/PEG-Mal (I-Gel) and PEG-SH/PEG-Mal/β-CD Hydrogels (H-Gel). For this purpose, four-armed PEG-Mal (20 K) and four-armed PEG-SH (20 K) were both dissolved in ddH₂O to a concentration of 7 mM. Then, two kinds of solutions were quickly mixed at a volume ratio of 1:1. The transparent PEG-SH/PEG-Mal hydrogels formed in seconds after mixing. For the preparation of PEG-SH/PEG-Mal/β-CD hydrogels, β-CD was dissolved in four-armed PEG-Mal solutions (7 mM). Then, the four-armed PEG-Mal/CD solution was mixed with four-armed PEG-SH solution at a volume ratio of 1:1, and PEG-SH/PEG-Mal/β-CD hydrogels were obtained. All the resulting hydrogels were dialyzed in ddH₂O for 24 h to remove β-CD and unreacted PEG.

IT-AFM Experiments. AFM experiments were carried out on a commercial AFM (JPK, Nanowizard II). The force curves were obtained and analyzed using commercial software from JPK. The D type MLCT (Bruker, Germany, with the half-open angle of the pyramidal face of α < 20°, tip radius: 20 nm) cantilever was chosen for the experiments. The spring constant of the cantilevers was 50 to 60 pN · nm⁻¹, which was calibrated prior to the measurements using the equipartition theorem in the solvent for each experiment. The maximum loading force was set to 300 pN. All AFM experiments were carried out at room temperature. In a typical experiment, the hydrogel was spread over the surface of the glass substrates in deionized water. Then, the cantilever was moved above the hydrogel with the help of positioning systems. The cantilever was brought to the samples with a constant speed of 2 μm · s⁻¹ until a loading force of 300 pN was reached. Then, the cantilever was retracted and moved to another spot for the next cycle. By fitting the approaching curve to the Hertz model (11), we obtained the Young's modulus values of the hydrogels. The indentation fitting was performed using the commercial data processing software provided by JPK. Typically, three to four such regions (5 μm × 5 μm, 1,600 pixels) were randomly selected on each sample to determine the average Young's modulus.

$$F(h) = \frac{2}{\pi}\tan\alpha\,\frac{E}{1-v^2}h^2,\qquad\qquad \textbf{[11]}$$

where F is the stress of the cantilever, h is the depth of the hydrogel pressed by the cantilever tip, α is the half angle of the tip (15°), E is the Young's modulus of the tissue, and v is the Poisson ratio. We chose v = 0.5 in our calculation.

hESC Culture and Differentiation on Hydrogels. hESCs were kindly provided by the Stem Cell Bank, Chinese Academy of Science, and labeled ESC H9. hESCs were expanded in mTeSR1 (STEMCELL Technologies) on Matrigel-coated (BD Biosciences) tissue culture plates, and mTeSR1 was replaced daily. All hMSCs were cultured for 2 d prior to the experiments.

For the cell culture of hESCs on hydrogels, 150-μL hydrogels were prepared on round coverslips (20 mm, WHB) in 12-well cell culture plates (Thermo). Cells seeded on glass substrate were used as the control group. Then, 2 mL of PBS (10 mM, pH = 7.4) was pipetted into each well, and the hydrogels were allowed to swell for 24 h before the PBS was removed. The swelling cycle was repeated four times. Then, the hESCs were seeded on the hydrogels at a density of 1×10^3 cell colonies per well in mTeSR1, and mTeSR1 was replaced daily. qPCR analysis was performed after 5 d and 10 d. Immunocytochemical staining was also performed after 10 d.

Immunostaining and Cell Morphology Analysis. For immunofluorescence, cells were fixed in 2% (volume/volume) paraformaldehyde for 30 min and then treated with 0.1% Triton X-100 for 15 min. After blocking in 5% (weight/volume) bovine serum albumin (BSA) for 1 h to minimize nonspecific binding, anti-Oct 3/4, anti-Sox2, and anti-YAP primary antibodies diluted with antibody dilution buffer were added to the fixed cells and incubated overnight at 4 °C. Then, the primary antibody solution was decanted, and the dish was immediately washed with PBS 3 × 5 min. After being rinsed with PBST (0.5 weight percentage Tween-20 in PBS) three times, the secondary antibody (goat anti-mouse Alexa Fluor 488; goat anti-mouse Alexa Fluor 594) in PBS was added to the dish, and the cells were incubated for 60 min at room temperature. Then, the secondary antibody was decanted, and the cells were washed with PBST 3 × 5 min. All images were obtained using a laser confocal fluorescence microscope (Olympus FV3000). For the images of hESCs on hydrogels at high ($C_{PEG-Mal} = C_{PEG-SH} = 105$ mg · mL^{-1})- and low-PEG ($C_{PEG-Mal} = C_{PEG-SH} = 52.5$ mg · mL^{-1}) concentrations, the images were obtained using a fluorescence microscope OLYMPUS-IX81 (OLYMPUS). Quantitative image analyses were performed using ImageJ.

qRT-PCR Analysis. Total RNA from cells was extracted using TRIzol reagent, and then 1,000 ng of total RNA was reverse transcribed into complementary ribonucleic acid (cDNA) with 5× PrimeScript RT Master Mix following the manufacturer's instructions. Real-time PCR was conducted using the SYBR Premix Ex TaqTM II kit (DRR081A, Takara Bio Inc.) on the LightCycler 96 system (Roche). The sense and antisense sequences of the primers used for quantitative RT-PCRs are summarized in *SI Appendix*, Table S1. The reaction was performed under the following conditions: incubation at 95 °C for 2 min; denaturation at 94 °C for 15 s, annealing at 58 °C for 15 s, and polymerization at 72 °C for 60 s for 40 cycles; and a final extension at 72 °C for 5 min. All cycle-threshold (C_t) values were analyzed quantitatively and normalized to their respective GAPDH values. The relative levels were calculated using the $2 - \Delta\Delta C_t$ method.

Statistical significance was determined using Student's *t* test or one-way ANOVA accordingly. Statistical significance was set to a *P* value <0.05.

Data Availability. All study data are included in the article and/or *SI Appendix*.

1. C. Bonnans, J. Chou, Z. Werb, Remodelling the extracellular matrix in development and disease. *Nat. Rev. Mol. Cell Biol.* **15**, 786–801 (2014).
2. A. J. Engler, S. Sen, H. L. Sweeney, D. E. Discher, Matrix elasticity directs stem cell lineage specification. *Cell* **126**, 677–689 (2006).
3. M. P. Lutolf, P. M. Gilbert, H. M. Blau, Designing materials to direct stem-cell fate. *Nature* **462**, 433–441 (2009).
4. P. M. Gilbert et al., Substrate elasticity regulates skeletal muscle stem cell self-renewal in culture. *Science* **329**, 1078–1081 (2010).
5. J. D. Humphrey, E. R. Dufresne, M. A. Schwartz, Mechanotransduction and extracellular matrix homeostasis. *Nat. Rev. Mol. Cell Biol.* **15**, 802–812 (2014).
6. G. Huang et al., Functional and biomimetic materials for engineering of the three-dimensional cell microenvironment. *Chem. Rev.* **117**, 12764–12850 (2017).
7. K. A. Kilian, B. Bugarija, B. T. Lahn, M. Mrksich, Geometric cues for directing the differentiation of mesenchymal stem cells. *Proc. Natl. Acad. Sci. U.S.A.* **107**, 4872–4877 (2010).
8. R. Oria et al., Force loading explains spatial sensing of ligands by cells. *Nature* **552**, 219–224 (2017).
9. H. Kang et al., An in situ reversible heterodimeric nanoswitch controlled by metal-ion-ligand coordination regulates the mechanosensing and differentiation of stem cells. *Adv. Mater.* **30**, e1803591 (2018).
10. A. M. Rosales, K. S. Anseth, The design of reversible hydrogels to capture extracellular matrix dynamics. *Nat. Rev. Mater.* **1**, 15012 (2016).
11. J. Du et al., Compression generated by a 3D supracellular actomyosin cortex promotes embryonic stem cell colony growth and expression of Nanog and Oct4. *Cell Syst.* **9**, 214–220.e5 (2019).
12. Y. Li et al., Compression-induced dedifferentiation of adipocytes promotes tumor progression. *Sci. Adv.* **6**, eaax5611 (2020).
13. Y. L. Han et al., Cell contraction induces long-ranged stress stiffening in the extracellular matrix. *Proc. Natl. Acad. Sci. U.S.A.* **115**, 4075–4080 (2018).
14. J. D. Boerckel, B. A. Uhrig, N. J. Willett, N. Huebsch, R. E. Guldberg, Mechanical regulation of vascular growth and tissue regeneration in vivo. *Proc. Natl. Acad. Sci. U.S.A.* **108**, E674–E680 (2011).
15. K. H. Vining, D. J. Mooney, Mechanical forces direct stem cell behaviour in development and regeneration. *Nat. Rev. Mol. Cell Biol.* **18**, 728–742 (2017).
16. A. K. Denisin, B. L. Pruitt, Tuning the range of polyacrylamide gel stiffness for mechanobiology applications. *ACS Appl. Mater. Interfaces* **8**, 21893–21902 (2016).
17. X. Wu et al., Reversible hydrogels with tunable mechanical properties for optically controlling cell migration. *Nano Res.* **11**, 5556–5565 (2018).
18. B. Xue et al., Electrically controllable actuators based on supramolecular peptide hydrogels. *Adv. Funct. Mater.* **26**, 9053–9062 (2016).
19. H. Wang, S. C. Heilshorn, Adaptable hydrogel networks with reversible linkages for tissue engineering. *Adv. Mater.* **27**, 3717–3736 (2015).
20. S. Naahidi et al., Biocompatibility of hydrogel-based scaffolds for tissue engineering applications. *Biotechnol. Adv.* **35**, 530–544 (2017).
21. H. Geckil, F. Xu, X. Zhang, S. Moon, U. Demirci, Engineering hydrogels as extracellular matrix mimics. *Nanomedicine (Lond.)* **5**, 469–484 (2010).
22. J. Xia, Y. Yuan, H. Wu, Y. Huang, D. A. Weitz, Decoupling the effects of nanopore size and surface roughness on the attachment, spreading and differentiation of bone marrow-derived stem cells. *Biomaterials* **248**, 120014 (2020).
23. T. Sakai et al., Design and fabrication of a high-strength hydrogel with ideally homogeneous network structure from tetrahedron-like macromonomers. *Macromolecules* **41**, 5379–5384 (2008).
24. M. Malkoch et al., Synthesis of well-defined hydrogel networks using click chemistry. *Chem. Commun. (Camb.)* **1**, 2774–2776 (2006).
25. B. D. Polizzotti, B. D. Fairbanks, K. S. Anseth, Three-dimensional biochemical patterning of click-based composite hydrogels via thiolene photopolymerization. *Biomacromolecules* **9**, 1084–1087 (2008).
26. J. A. Hubbell, Synthetic biodegradable polymers for tissue engineering and drug delivery. *Curr. Opin. Solid State Mater. Sci.* **3**, 246–251 (1998).
27. A. Metters, J. Hubbell, Network formation and degradation behavior of hydrogels formed by Michael-type addition reactions. *Biomacromolecules* **6**, 290–301 (2005).
28. Y. Park, M. P. Lutolf, J. A. Hubbell, E. B. Hunziker, M. Wong, Bovine primary chondrocyte culture in synthetic matrix metalloproteinase-sensitive poly(ethylene glycol)-based hydrogels as a scaffold for cartilage repair. *Tissue Eng.* **10**, 515–522 (2004).
29. H. J. Lee, G. M. Fernandes-Cunha, D. Myung, In situ-forming hyaluronic acid hydrogel through visible light-induced thiol-ene reaction. *React. Funct. Polym.* **131**, 29–35 (2018).
30. J. Collins, Z. Xiao, M. Müllner, L. A. Connal, The emergence of oxime click chemistry and its utility in polymer science. *Polym. Chem-UK* **7**, 3812–3826 (2016).
31. E. A. Phelps et al., Maleimide cross-linked bioactive PEG hydrogel exhibits improved reaction kinetics and cross-linking for cell encapsulation and in situ delivery. *Adv. Mater.* **24**, 64–70, 2 (2012).
32. B. H. Northrop, R. N. Coffey, Thiol-ene click chemistry: Computational and kinetic analysis of the influence of alkene functionality. *J. Am. Chem. Soc.* **134**, 13804–13817 (2012).
33. D. P. Nair et al., The Thiol-Michael addition click reaction: A powerful and widely used tool in materials chemistry. *Chem. Mater.* **26**, 724–744 (2014).
34. J. Kim et al., Characterization of the crosslinking kinetics of multi-arm poly(ethylene glycol) hydrogels formed via Michael-type addition. *Soft Matter* **12**, 2076–2085 (2016).
35. R. Cruz-Acuña et al., PEG-4MAL hydrogels for human organoid generation, culture, and in vivo delivery. *Nat. Protoc.* **13**, 2102–2119 (2018).
36. A. J. García, PEG-maleimide hydrogels for protein and cell delivery in regenerative medicine. *Ann. Biomed. Eng.* **42**, 312–322 (2014).
37. C. T. Johnson et al., Hydrogel delivery of lysostaphin eliminates orthopedic implant infection by *Staphylococcus aureus* and supports fracture healing. *Proc. Natl. Acad. Sci. U.S.A.* **115**, E4960–E4969 (2018).

8 of 9 | **PNAS**
https://doi.org/10.1073/pnas.2110961118

Xue et al.
Engineering hydrogels with homogeneous mechanical properties for controlling stem cell lineage specification

38. N. J. Darling, Y.-S. Hung, S. Sharma, T. Segura, Controlling the kinetics of thiol-maleimide Michael-type addition gelation kinetics for the generation of homogenous poly(ethylene glycol) hydrogels. *Biomaterials* **101**, 199–206 (2016).

39. L. E. Jansen, L. J. Negrón-Piñeiro, S. Galarza, S. R. Peyton, Control of thiol-maleimide reaction kinetics in PEG hydrogel networks. *Acta Biomater.* **70**, 120–128 (2018).

40. R. McLemore, S. A. Robb, B. H. Lee, M. R. Caplan, B. L. Vernon, Michael-type addition reactions in NIPAAm-cysteamine copolymers follow second order rate laws with steric hindrance. *Ann. Biomed. Eng.* **37**, 2416–2425 (2009).

41. M. P. Lutolf, N. Tirelli, S. Cerritelli, L. Cavalli, J. A. Hubbell, Systematic modulation of Michael-type reactivity of thiols through the use of charged amino acids. *Bioconjug. Chem.* **12**, 1051–1056 (2001).

42. E. P. Chan, E. J. Smith, R. C. Hayward, A. J. Crosby, Surface wrinkles for smart adhesion. *Adv. Mater.* **20**, 711–716 (2008).

43. S. P. Zustiak, H. Boukari, J. B. Leach, Solute diffusion and interactions in cross-linked poly(ethylene glycol) hydrogels studied by fluorescence correlation spectroscopy. *Soft Matter* **6**, 3609–3618 (2010).

44. F. Yhaya *et al.*, Development of micellar novel drug carrier utilizing temperature-sensitive block copolymers containing cyclodextrin moieties. *Macromolecules* **44**, 8433–8445 (2011).

45. A. Charlot, R. Auzély-Velty, Novel hyaluronic acid based supramolecular assemblies stabilized by multivalent specific interactions: Rheological behavior in aqueous solution. *Macromolecules* **40**, 9555–9563 (2007).

46. A. Harada, Y. Takashima, M. Nakahata, Supramolecular polymeric materials via cyclodextrin-guest interactions. *Acc. Chem. Res.* **47**, 2128–2140 (2014).

47. M. V. Rekharsky, Y. Inoue, Complexation thermodynamics of cyclodextrins. *Chem. Rev.* **98**, 1875–1918 (1998).

48. L. Li *et al.*, Polymer networks assembled by host–guest inclusion between adamantyl and β-cyclodextrin substituents on poly(acrylic acid) in aqueous solution. *Macromolecules* **41**, 8677–8681 (2008).

49. Y. S. Su, J. W. Liu, Y. Jiang, C. F. Chen, Assembly of a self-complementary monomer: Formation of supramolecular polymer networks and responsive gels. *Chemistry* **17**, 2435–2441 (2011).

50. V. Hong, A. A. Kislukhin, M. G. Finn, Thiol-selective fluorogenic probes for labeling and release. *J. Am. Chem. Soc.* **131**, 9986–9994 (2009).

51. C. K. Riener, G. Kada, H. J. Gruber, Quick measurement of protein sulfhydryls with Ellman's reagent and with 4,4′-dithiodipyridine. *Anal. Bioanal. Chem.* **373**, 266–276 (2002).

52. C. Yang *et al.*, Spatially patterned matrix elasticity directs stem cell fate. *Proc. Natl. Acad. Sci. U.S.A.* **113**, E4439–E4445 (2016).

53. M. J. Dalby, N. Gadegaard, R. O. Oreffo, Harnessing nanotopography and integrin-matrix interactions to influence stem cell fate. *Nat. Mater.* **13**, 558–569 (2014).

54. M. J. Dalby *et al.*, The control of human mesenchymal cell differentiation using nanoscale symmetry and disorder. *Nat. Mater.* **6**, 997–1003 (2007).

55. S. Oh *et al.*, Stem cell fate dictated solely by altered nanotube dimension. *Proc. Natl. Acad. Sci. U.S.A.* **106**, 2130–2135 (2009).

56. K. Ye *et al.*, Matrix stiffness and nanoscale spatial organization of cell-adhesive ligands direct stem cell fate. *Nano Lett.* **15**, 4720–4729 (2015).

Xue et al.
Engineering hydrogels with homogeneous mechanical properties for controlling stem cell lineage specification

PNAS | 9 of 9
https://doi.org/10.1073/pnas.2110961118